Time-resolved high-harmonic spectroscopy of the photodissociation of CH3I and CF3I

Author(s):
Tehlar, Andres; Wörner, Hans Jakob

Publication date:
2013

Permanent link:
https://doi.org/10.3929/ethz-a-010779553

Originally published in:
Molecular Physics 111(14-15), https://doi.org/10.1080/00268976.2013.782439

Funding acknowledgement:
128274 - Attosecond imaging of chemical dynamics (SNF)

To appear in *Molecular Physics*
Vol. 00, No. 00, Month 200x, 1–15

RESEARCH ARTICLE

Time-resolved high-harmonic spectroscopy of the photodissociation of CH_3I and CF_3I

A. Tehlar and H.J.Wörner*

Laboratorium für physikalische Chemie, Wolfgang-Pauli-Str. 10, ETH Zürich, CH-8093 Zürich, Switzerland

(*Received 00 Month 200x; final version received 00 Month 200x*)

The photodissociation dynamics of iodomethane (CH_3I) and trifluoroiodomethane (CF_3I) have been studied using time-resolved high-harmonic spectroscopy. The molecules were photoexcited in a transient grating geometry to their respective A bands by laser pulses centered at 267 nm and were probed through high-harmonic generation driven by a delayed 800 nm laser pulse. Both molecules display a fast buildup of the diffracted high harmonics (H9-H15) followed by a slower decay, while the undiffracted harmonics exhibit an opposite modulation. The time scales on which the signals reach their asymptotic values were found to be slower in CF_3I compared to CH_3I and to weakly increase with high-harmonic order in both molecules. In the case of CH_3I the obtained time scales are in agreement with dissociation times measured by other techniques. Our results on CF_3I constitute the first time-resolved measurements of the A-band dissociation. A simple theoretical model for the variation of the harmonic phase induced by the changing vertical ionisation potential is combined with one-dimensional nuclear wave packet propagation and shown to qualitatively account for the main observations.

Keywords: High-Harmonic Generation; High-Harmonic Spectroscopy; Transient-grating spectroscopy; Iodomethane; Trifluoroiodomethane; CH3I; CF3I;

1. Introduction

Chemical reactions are the result of the concerted dynamics of valence electrons and atomic motions. Obtaining a detailed understanding of these fundamental phenomena requires the development of methods that offer simultaneously a high temporal resolution and a high sensitivity to the structure of the valence shell. Important progress has been made in recent years through the technique of high-harmonic generation that provides attosecond pulse trains in the extreme ultraviolet (XUV). The generation of isolated attosecond pulses has driven the development of several time-resolved techniques [1–3]. The isolation of single high-harmonic orders has made time-resolved photoelectron spectroscopy in the XUV possible [4, 5]. In addition to being a promising source of radiation, high-harmonic generation can also be used as a technique to investigate the structure and dynamics of the generating medium. This application, which is known as high-harmonic spectroscopy (HHS), has been used to study the dynamics of molecules initially prepared in their electronic ground state. The non-resonant excitation of rotational and vibrational wave packets has been exploited to characterise the high-harmonic emission of molecules as a function of their spatial orientation [6–12] or as a function of vibrational displacements [13, 14], respectively. These experiments, among many others, have

*Corresponding author. Email: woerner@phys.chem.ethz.ch, web: www.atto.ethz.ch

ISSN: 0040-5167 print/ISSN 1754-2278 online

DOI: 10.1080/0040516YYxxxxxxxx
http://www.informaworld.com

revealed the sensitivity of high-harmonic generation to the electronic structure of molecules. Applying HHS to electronically excited states supporting photochemical dynamics has however remained a challenge because of the low excitation fractions typical for femtosecond time-resolved experiments. Recently, we have introduced time-resolved HHS (TRHHS) and have shown that the technique offers a natural solution to the problem of weak excitations [15, 16]. The high-harmonic emissions from all species present in the sample are phase-locked to the generating laser field. This situation results in a coherent detection of the weak emissions from transient species against the strong background provided by the unexcited molecules, resulting in a high sensitivity. Combined with the transient grating technique [17–19], both amplitude and phase of the emission can be measured [10, 15], providing detailed insight into the structure and dynamics of molecules. Time-resolved high-harmonic spectroscopy has been applied so far to the photodissociation of Br_2 [15, 16] and to non-adiabatic dynamics at conical intersections in NO_2 [20, 21].

The general principles and the specificities of TRHHS have been outlined and analysed recently [22]. This work showed that the signals measured in TRHHS reflect two complementary aspects of excited-state dynamics. In adiabatic dynamics, taking place on a single potential energy surface, the temporal variation of the high-harmonic emission reflects the changing electronic structure of the excited-state wave packet and the variation of the vertical ionisation energy. In non-adiabatic dynamics involving intersections of multiple electronic potential energy surfaces, the population dynamics contribute to the observed signal in addition to the temporal variation resulting from wave-packet motion. Since the photodissociation dynamics of polyatomic molecules is in general complex, further experiments are desirable to reach a better understanding of the principles, the potential and the limitations of the method.

In this article, we study the photodissociation of CH_3I following excitation to the A-band and compare the results with those of other methods. In addition, we study CF_3I which is known to have similar dissociative electronic states but for which no time scale for the A-band photodissociation dynamics of CF_3I has been reported. The knowledge about the photochemical dynamics of these molecules dates back to the discovery of the first laser relying on photodissociation by Kasper and Pimentel in 1964 [23]. Lasing was observed at 1.3 μm as a consequence of population inversion in the fine-structure levels of the atomic iodine photofragment. A detailed study using velocity-map imaging of the fragments showed that photoexcitation at 267 nm prepares almost exclusively the $^3Q_{0^+}$ state in a parallel transition. This state correlates with the CH_3 + I($^2P_{1/2}$) channel and has an intersection with the $^1Q_1$ state that is weakly populated through a non-adiabatic transition, yielding a small population in the CH_3 + I($^2P_{3/2}$) channel [24].

The first time-resolved measurements on methyl iodide were performed by Zhong and Zewail in 1998 using the kinetic-energy time-of-flight (KETOF) method. They obtained a dissociation time of 125 fs, defined as the appearance time of the methyl fragment which was detected through resonance-enhanced multiphoton ionisation (REMPI) [25]. Recently, Bañares and co-workers studied the photodissociation of methyl iodide by combining REMPI with velocity-map-imaging detection of the fragments, allowing them to resolve the dissociation times of the methyl fragments associated with each of the two dissociation channels. They obtained appearance times of 80±20 fs for the CH_3 + I($^2P_{1/2}$) channel and 40±20 fs for the CH_3 + I($^2P_{3/2}$) channel [26]. In a complementary experiment, the same group used multiphoton ionisation to probe the dissociation dynamics. Since this detection method is non-resonant, it gives access to the temporal evolution of the transient photoexcited species. Using non-resonant strong-field ionisation, delayed maxima in the

fragment ion yields and exponential decay times of 50±20 fs for the CH_3^+ signal and 40±20 fs for the I^+ signal were obtained [27]. Time-resolved studies of the intramolecular vibrational dynamics of CH_3I have been reported by Quack et al. both in the gas phase and in solution showing that ultrafast vibrational energy redistribution is governed by three different time scales [28, 29].

In the case of CF_3I, the time scale of dissociation following excitation to the A band has not been reported but a time span of 150-350 fs has been estimated from the anisotropy factor of the photofragments [30]. In addition several simultaneously occurring multiphoton processes related to the A-band photodissociation have been observed [31]. Time-resolved studies have also been performed on the dynamics of Rydberg states accessed through multiphoton excitation [32]. The photodissociation of CF_3I induced by multiphoton absorption at 10 μm has also been studied and the populations of fine- and hyperfine levels of the iodine photofragment have been measured by high-resolution diode laser spectroscopy (see [33] and references therein).

2. Method

2.1. *Experiment*

The experimental setup consisted of an amplified Ti:sapphire laser system, generating 25 fs laser pulses centred at 800 nm with a repetition rate of 1 kHz and a vacuum chamber for the generation and characterisation of extreme-ultraviolet (XUV) high-harmonic radiation. The output of the laser system was separated into a pump and a probe beam using a beam splitter. The pump pulses were generated by frequency tripling the 800 nm laser pulses. This was achieved by frequency-doubling the 800 nm laser beam in a beta-barium borate (BBO) crystal, compensating the group delay of the emerging 400 nm pulses with respect to the 800 nm pulses by means of a calcite plate, rotating the polarisations of the 800 and 400 nm pulses into the same plane using a zero-order $\lambda/2$-waveplate at 800 nm (i.e. λ at 400 nm), and performing the sum-frequency mixing (800+400 nm) in a second BBO crystal. The 267 nm pulses were reflected on two lowpass dichroic mirrors to separate the remaining 400 nm and 800 nm radiation. The 267 nm beam was split into two beams of equal intensity using a 50:50 beamsplitter. One of the two beams was sent over a translation stage that controlled the delay between the two pulses. The beams were subsequently aligned parallel to each other and to the 800 nm probe beam with which they were recombined using a lowpass dichroic mirror. A vertical distance of $\sim \pm 1$ cm between the central probe beam and the vertically displaced pump beams was chosen, as illustrated in Fig. 1.

The time delay Δt between the pump and probe pulses was controlled by a motorised delay stage. All three beams were focused into the experimental chamber using a single $f = 45$ cm spherical aluminum mirror. The angle of $\sim$1.5° between the pump beams created a vertically-modulated transient grating in the focus with a spatial periodicity Λ of about 10 μm. Typical energies of the pump pulses were around 10 μJ, the high-harmonic-generating probe pulse had energies around 0.9 mJ. A General Valve operating at a repetition rate of 100 Hz with a backing pressure of 4 bar was used to generate a cold supersonic gas expansion of the investigated molecules into vacuum. Helium was bubbled through liquid CH_3I held at room temperature whereas the gaseous CF_3I was premixed with He in a ratio of 1:5. Higher dilution of the samples led to a significant deterioration of the signal because of the quadratic dependence of the high-harmonic generation signal on the target density. The synchronisation between laser and gas pulses was chosen

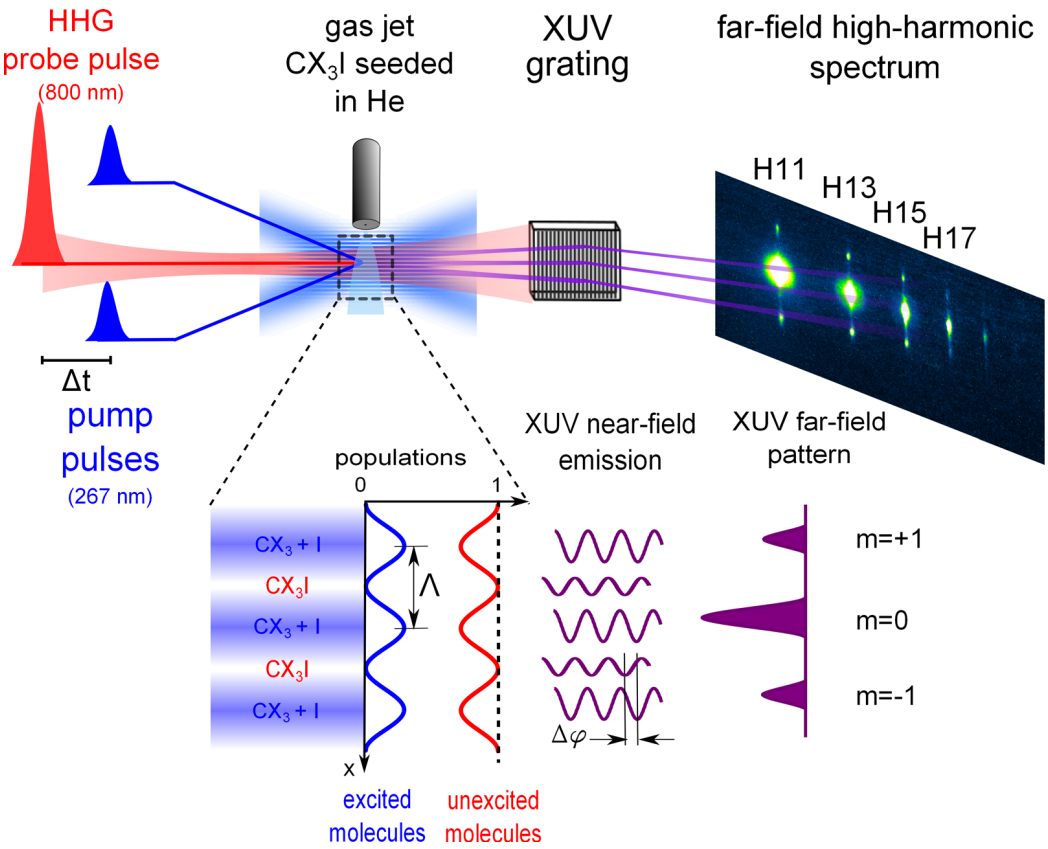

Figure 1. Schematic representation of the experimental setup: Two synchronised pump pulses centered at 267 nm cross at their focus, where they generate an intensity grating that induces a spatial modulation of the excited population of the CX_3I (X = H, F) molecules. The delayed probe pulse generates high harmonics in the structured sample, resulting in a modulation of the amplitude and phase of the near-field emission which causes diffraction in the far field. The high-harmonic emission is spectrally dispersed using an XUV grating and detected in the far field. When the pump pulses precede the probe pulse, first-order diffraction ($m = \pm 1$) is observed in the far field in addition to the undiffracted radiation ($m = 0$). (See text for additional information on the setup).

such that the early part of the supersonic expansion was probed to minimize the presence of clusters. The rotational cooling was optimised and the cluster formation was further suppressed by adjusting the experimental conditions such as to optimise the contrast of the rotational revivals following impulsive alignment of CH_3I [34]. A cylindrical XUV grating spectrally dispersed the high-harmonic emission in the horizontal plane while allowing free propagation in the vertical direction (see Fig. 1). The spectrally-resolved far-field high-harmonic profiles were acquired using a microchannel-plate (MCP) detector coupled to a phosphor screen.

2.2. *Data Analysis*

Typical spectrally resolved far-field harmonic profiles are displayed in Fig. 2. At negative delays, i.e. when the probe pulse precedes the pump pulses, the regular odd harmonics H9–H21 are observed (Fig. 2a). As in previous publications, this undiffracted radiation is designated as $m = 0$, the zeroth order of the transient grating. At zero delay, i.e. when the pump and probe pulses temporally overlap, four additional vertically displaced sidebands appear, two above and two below each harmonic order (Fig. 2b). The two peaks closest to $m = 0$ originate from wave mixing between the 267 nm pump pulses and the 800 nm probe pulse. We therefore designate them as $wm = \pm 1$. Conservation of the linear photon momenta, energies and total parity dictates the position where this emission appears on the

detector. Following Ref. [35], these emissions can be labeled by (n_1, n_2) according to the net numbers n_1 of 800 nm photons and n_2 of 267 nm photons that are involved in their generation. The emissions highlighted by the boxes in Fig. 2b correspond to (10,1) and (16,-1), where each process contributes to both spots depending on which of the two pump pulses is involved in the generation process. The two weaker spots located outside the boxes have contributions from both wave mixing (7,2) and (19,-2), as well as diffraction resulting from the molecular excitation grating. At positive pump-probe delays (Fig. 2c), diffraction form the transient grating ($m = \pm 1$) is the only contributor to this emission that is highlighted by boxes in Fig. 2c. In the present experiments, as in previous ones [15, 20, 21, 35], we have found that wave mixing is strongly suppressed for perpendicular polarisations of pump and probe pulses. For sufficiently low intensities of the excitation pulses the contribution of wave mixing to the diffracted radiation can therefore be neglected. This is not the case in parallel polarisations, where wave mixing is always observed as a strong contribution. The signal intensity as a function of the pump-probe delay traces was obtained by selecting the areas corresponding to these different optical processes in the acquired far-field high-harmonic spectra.

Since no transient grating is present for negative time delays, the intensity in the $m = \pm 1$ regions is expected to be zero before the arrival of the pump pulses. Thus, the average of the integrated intensity in these areas was treated as constant background and subtracted from the signal. The integrated intensities of all five emission maxima in each harmonic order ($m = 0, \pm 1$; $wm = \pm 1$) were normalised with respect to the signal measured in $m = 0$ at negative time delays. The wave-mixing signal provides the cross-correlation signal and zero delay time. Since the $wm = \pm 1$ spots partially overlap with the $m = 0$ emission and the wave-mixing signal is mainly a cross-correlation signal with vanishing intensities at both large negative and large positive Δt, the signal in $m = 0$ was appropriately subtracted from that in $wm = \pm 1$. The fit parameters presented in Table 1 are weighted means over several experimental scans using the inverse of their absolute error intervals as weight. The error intervals given in Table 1 correspond to the weighted standard deviation of the measurements.

3. Results

Figure 3 shows the experimental results obtained on the photodissociation of CH_3I. The molecules were excited using ∼50-70 fs pulses centered at 267 nm and high-harmonic generation was performed by a delayed 30 fs pulse centered at 800 nm. The black curves show the intensity of the undiffracted radiation ($m = 0$) at harmonics 9 to 15 as a function of the pump-probe delay. The red curves show the intensity in the first-order diffraction sideband $m = \pm 1$, and the blue curve shows the signal resulting from wave mixing between the 800 and 267 nm pulses during their temporal overlap [35]. All signals have been normalised to the intensity at negative delays in $m = 0$ of the same harmonic order, which corresponds to high-harmonic emission from molecules in the electronic ground state only. also normalized to the emission of the unexcited molecules. As discussed in the previous section, the wave-mixing signal is spatially separated from both the undiffracted and the diffracted radiation and can thus be measured separately. This feature provides an *in-situ* calibration of the zero pump-probe delay and a measurement of the cross-correlation time of the experiment.

The temporal evolution of the signal is qualitatively similar across the observed harmonic orders. The undiffracted signal ($m = 0$) is found to decrease following photoexcitation in all harmonic orders. This behavior has been observed also in all

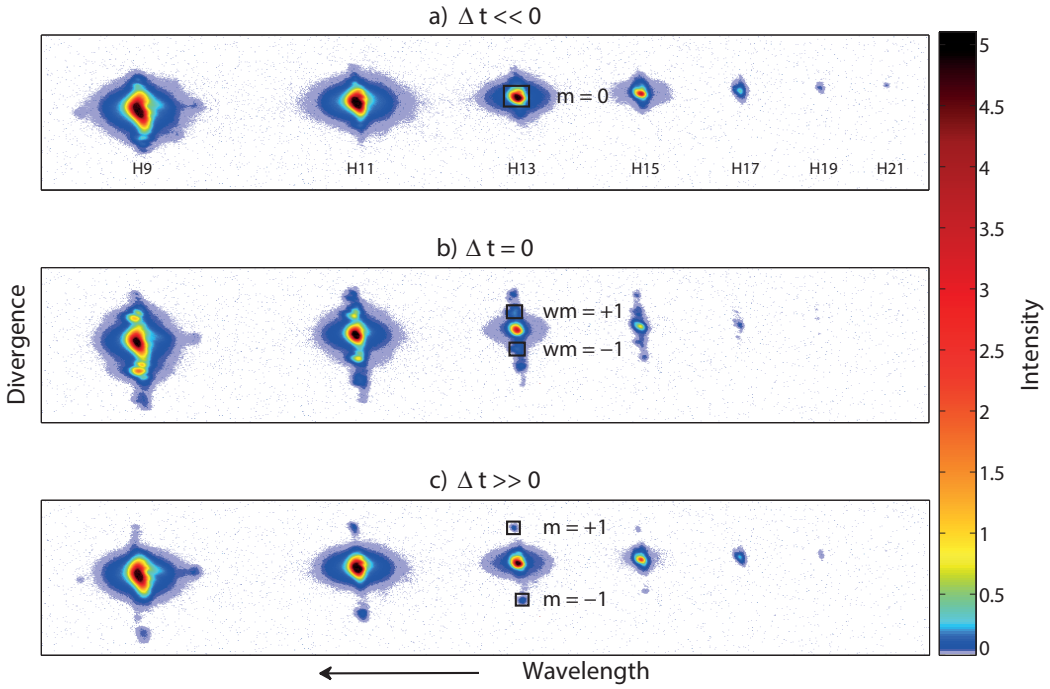

Figure 2. Typical far-field high-harmonic profiles obtained at different time delays. The color coding of the intensity is shown on the right (colored figure in the electronic version). a) At negative time delays (probe before pump pulses), only undiffracted high-harmonic emission is observed. The analysis area of $m = 0$ for H13 is shown. b) Around $\Delta t = 0$, the interaction of the probe with each of the pump pulses leads to additional emission in the $wm = \pm 1$ and $m = \pm 1$ spots. The $wm = \pm 1$ areas are shown in red for H13. c) At large positive time delays, the $m = \pm 1$ emission (highlighted areas for H13) results from the presence of a transient grating in the sample.

previous experiments using TRHHS and has been shown to originate from partially destructive interference of high-harmonic emissions from excited and unexcited molecules [16]. The undiffracted signal partially recovers after the initial decrease. The depth of the signal modulation increases with harmonic order. The signal in the diffraction sidebands ($m = \pm 1$) increases during the photoexcitation process and subsequently decays. The maximal value reached by the normalised signals also increases with high-harmonic order. We note that Fig. 3 only shows the early part of the dissociation dynamics but our measurements include several data sets extending to delay times of 1.5 ps which were important in determining reliable exponential time constants in our model. This is also the case for the CF_3I measurements.

Figure 4 shows the experimental results obtained on the photodissociation of CF_3I using identical conditions as for the studies of CH_3I. To our knowledge, these results are the first time-resolved measurements of the photodissociation of CF_3I from the A band. The temporal variation of the signals is qualitatively similar to the observations in CH_3I although the modulations are slower in the case of CF_3I. This observation is consistent with the expected slower dissociation dynamics of a heavier molecule when potential energy surfaces of similar shape are involved.

The variation of all observed $m = 0$ signals appears to be well described by a fast drop followed by a slow recovery. All $m = \pm 1$ signals display a fast buildup followed by a slow decay. We therefore choose the simplest possible model to describe the data and extract time constants. The temporal evolution of the diffracted signal is represented by a function that exponentially decays to an asymptotic value, convoluted with a Gaussian function

$$I_{m=\pm 1} = \left[\theta\left(t - t_e\right) \cdot \left(a + b \cdot \exp\left(-(t - t_e)/\tau\right)\right)\right] * \exp\left(-t^2/(2\sigma^2)\right), \qquad (1)$$

where θ is the heaviside step function, a and b represent signal amplitudes, τ is the time constant of the exponential decay, t_{e} is the temporal origin of the exponential function and σ is the width parameter of the Gaussian function. The normalised signal in $m = 0$ is represented by a similar function subtracted from one:

$$I_{m=0} = \left[1 - \theta\left(t - t'_{\mathrm{e}}\right) \cdot \left(a' + b' \cdot \exp\left(-(t - t'_{\mathrm{e}})/\tau'\right)\right)\right] * \exp\left(-t^2/(2\sigma'^2)\right). \quad (2)$$

These functions represent a purely phenomenological model that is used in the present work to extract apparent time constants from the measurements. They cannot be directly compared with those of the actual physical model, outlined in the following section, that relates the time-dependent properties of the molecule to the emitted high-harmonic radiation. We have however verified that the functions given by Eqs. (1) and (2) provide an excellent fit of the theoretical results described in the following section. Fitting Eqs. (1) and (2) to the theoretical results showed that the time constants $\tau(')$ and $\sigma(')$ depend on both m and the harmonic order. The time constants τ and σ as well as the amplitude factors were therefore all optimised independently. Attempts of reproducing the experimental data with a smaller number of free parameters, e.g. $t_e = t'_e = 0$ or $t_e = t'_e$ or order-independent time constants were not successful. The same holds true for the theoretical results discussed below. This aspect is further discussed in section 5.

The curves corresponding to the results of a non-linear least-squares fitting procedure of the model functions given by Eqs. (1) and (2) to the experimental data are shown in the Figs. 3 and 4. The agreement of the fitted curves with the experimental data shows that the results are well characterised by our model functions. Table 1 lists the average time constants obtained from 4–5 independent measurements.

The exponential time constants τ obtained for $m = 0$ and $m = \pm 1$ of a given harmonic order are found to agree within one standard deviation, although the time constants for $m = \pm 1$ appear to be slightly larger than those for $m = 0$. The time constants for both $m = 0$ and $m = \pm 1$ are found to increase with increasing harmonic order. All τ's obtained from fits to $m = 0$ lie within the error margin of any of the other harmonic orders. In $m = 1$ however, the error bars are smaller, indicating a systematic increase of exponential time constants with harmonic order. Similar trends in τ are also observed for the CF_3I results, where the time constants τ are found to increase with increasing harmonic order but they all overlap within one standard deviation. The temporal offset t_e of the exponential functions for both CH_3I and CF_3I are all negative but small and lie within the width of the cross-correlation function. The widths of the Gaussian function σ are found to be practically constant over the harmonic orders, in both diffracted and undiffracted radiation and for both molecules.

4. Theoretical model

The A band in the photoabsorption spectrum of CH_3I arises from three overlapping electronic transitions that connect the ground state to the $^3Q_1$, $^3Q_{0^+}$ and $^1Q_1$ states [36, 37]. The largest contribution comes from a parallel transition to the $^3Q_{0^+}$ state that dominates absorption at 267 nm. The perpendicular transitions to the $^3Q_1$ and $^1Q_1$ states represent less than 1 % of the absorption strength [38]. Photoexcitation thus mainly accesses the $^3Q_{0^+}$ state that correlates with atomic iodine in the $^2P_{1/2}$ state. Following excitation at 267 nm, about 10% of the excited population undergoes a non-adiabatic transition to the $^1Q_1$ state, forming iodine atoms in the $^2P_{3/2}$ state [26].

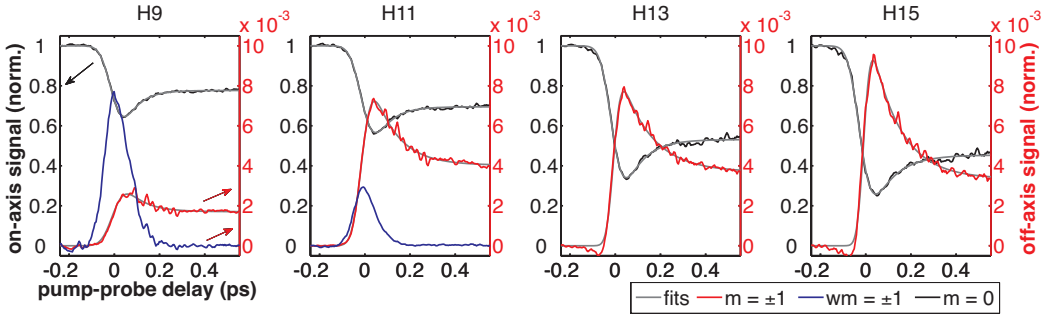

Figure 3. High-harmonic transient grating results on the photodissociation of CH_3I following excitation at 267 nm. High-harmonic generation was performed by an 800 nm laser pulse polarised perpendicularly to the excitation pulses. The four panels show the measured signals in several harmonic orders of $m = 0$ (left scale) and the averaged signals of $m = \pm 1$ and $wm = \pm 1$ (right scale), normalised to the signal in $m = 0$ at negative delays. Fitted curves according to Eqs. (1) and (2) for the $m = 0$ and $m = \pm 1$ traces are shown as thin grey lines.

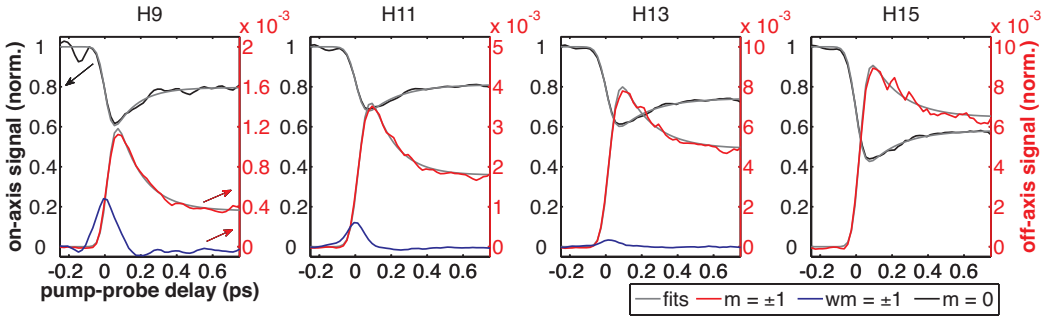

Figure 4. Same as Fig. 3 but for CF_3I.

Table 1. Fit parameters extracted from the experimental data on CH_3I and CF_3I for undiffracted ($m = 0$) and diffracted ($m = \pm 1$) high-harmonic signals using Eqs. (1) and (2). The error intervals indicate the standard deviation of four (CH_3I and those marked with *) respectively five (remaining CF_3I data) measurements. The origin of time is defined by the maximum wave mixing signal ($wm = \pm 1$) at harmonic 11.

Harmonic No.	CH_3I		CF_3I	
	$\tau_{m=0}$ / fs	$\tau_{m=\pm1}$ / fs	$\tau_{m=0}$ / fs	$\tau_{m=\pm1}$ / fs
9	91±40	101±16	164±31	146±25
11	105±51	119±31	185±30	162±30
13	117±57	149±36	193±41	231±104
15	125±56	136±34	211±68*	234±178*
	$t_{e,m=0}$ / fs	$t_{e,m=\pm1}$ / fs	$t_{e,m=0}$ / fs	$t_{e,m=\pm1}$ / fs
9	-19±9	-11±6	-14±19	-7±15
11	-21±9	-17±7	-5±16	-3±19
13	-25±12	-17±10	-11±19	0±19
15	-32±11	-16±8	-18±26*	4±20*
	$\sigma_{m=0}$ / fs	$\sigma_{m=\pm1}$ / fs	$\sigma_{m=0}$ / fs	$\sigma_{m=\pm1}$ / fs
9	43±10	41±8	44±7	30±4
11	45±15	39±17	44±6	36±3
13	45±20	33±26	43±4	37±4
15	46±20	30±23	43±4*	36±5*

We have recently formulated general expressions relating the properties of a time-dependent excited-state wave packet to the intensities of high-harmonic emission in both collinear and in transient-grating geometries [21]. The total wave function of a photoexcited molecule can be written in terms of a sum of products of electronic wave functions ϕ and nuclear wave functions χ of the electronic ground state (g)

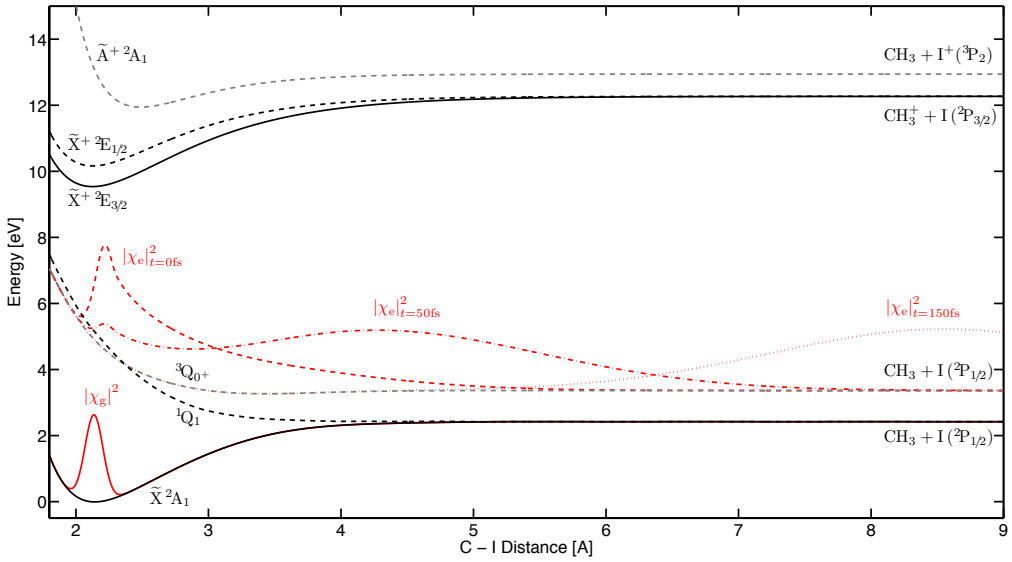

Figure 5. Relevant potential energy surfaces of CH_3I and CH_3I^+ as a function of the C-I distance (the main dissociation coordinate). The neutral states were taken from quantum chemical *ab initio* calculations reported in Refs. [39] and [40]. The cationic states were constructed using a Morse potential for a pseudo-diatomic molecule. The $\widetilde{X}^+$ states were modeled with the equilibrium distance $R_{eq} = 2.126$ Å [41], the ground state vibrational wavenumber $\tilde{\nu}_0 = 478.0$ cm^{-1} [42], the dissociation energy $D_e = 2.731$ eV [43], the adiabatic ionisation energy $I_P = 9.538$ eV [44] to the $\widetilde{X}^+\ ^2E_{3/2}$ state and the spin-orbit splitting of 5050 cm^{-1} [45]. The parameters $\tilde{\nu}_0 = 296.3$ cm^{-1}, $D_e = 0.925$ eV, the zero point energy $T_e = 11.944$ eV (all from [45]) and $R_{eq} = 2.503$ Å [41] were used for the $\widetilde{A}^+$ state. The curve crossings of the ionic potential energy surfaces shown in Ref. [46] were not taken into account because our present model is limited to strong-field ionisation to the $\widetilde{X}^+$ ground state of the cation.

and a set of electronically excited states (i)

$$\Psi(\mathbf{r},\mathbf{R},t) = c_g(t)\phi_g(\mathbf{r};\mathbf{R})\chi_g(\mathbf{R}) + \sum_i c_i(t)\phi_i(\mathbf{r};\mathbf{R})\chi_i(\mathbf{R},t), \tag{3}$$

where $\mathbf{r}$ and $\mathbf{R}$ represent the electronic and nuclear coordinates, respectively, and t is the time elapsed since photoexcitation. The excited state fraction r is given by the coefficients of the superposition state $r = 1 - |c_g|^2 = \sum_i |c_i|^2$ and $|c_i|^2 = r_i$. Atomic units are used in this section unless otherwise indicated. The electric field describing high-harmonic emission from this superposition state, that is assumed to evolve on a time scale t much slower than the period of the laser-field oscillation, is given by a coherent sum of the XUV radiation emitted from the different electronic states [21]

$$E_{\mathrm{XUV}}(\Omega,t) = (1 - r(t))\tilde{d}_g(\Omega) + \sum_i r_i(t)\tilde{d}_i(\Omega,t), \tag{4}$$

where $\tilde{d}_i(\Omega,t)$ is the time-dependent complex spectral representation of high-harmonic emission at photon energy Ω for the neutral molecular wave packet in the electronic state i. The $\tilde{d}_i(\Omega,t)$ can be calculated for each wave packet in a diabatic electronic basis as [21]

$$\tilde{d}_i(\Omega,t) = \int \mathrm{d}\mathbf{R}|\chi_i(\mathbf{R},t)|^2 \sum_f \sqrt{I^{if}(\mathbf{R})} d_r^{if}(\mathbf{R},\Omega) e^{-i\phi_{\mathrm{tot}}(\mathbf{R},\Omega)}, \tag{5}$$

where the sum runs over the accessible states f of the cation. I^{if} is the rate of

strong-field ionisation from the neutral state i to the cation state f, I_p^{if} the corresponding ionisation potential and d_r^{if} the corresponding complex photorecombination matrix element. Since both I^{if} and d_r^{if} depend on the molecular orientation with respect to the polarisation of the generating laser pulse, we use here the product $\sqrt{I^{if}(\mathbf{R})}d_r^{if}(\mathbf{R},\Omega)$ which we assume to have been averaged over the relevant molecular axis distribution. The term $e^{-i\phi_{\rm tot}(\mathbf{R},\Omega)}$ arises from the propagation of the electronic wave packet in the laser field [47, 48]. The phase $\phi_{\rm tot}(\mathbf{R},\Omega)$ accumulated during high-harmonic generation from an electronically excited state relative to the ground state can be approximated by $(I_p^{if}(\mathbf{R}) - I_p^g)\tau(\Omega)$ when $\Omega \gg I_p$ [48]. Since low harmonic orders are measured in the present work, we rather use the complete expression for the high-harmonic phase for each state [47]. On this basis, assuming a δ-like probe pulse, the intensities of high-harmonic emission in $m = 0$ and $m = \pm 1$ can be calculated as follows

$$I_{m=0}(\Omega,t) = \left|(1-r(t))\tilde{d}_g(\Omega) + \sum_i r_i(t)\tilde{d}_i(\Omega,t)\right|^2 \tag{6}$$

$$I_{m=\pm1}(\Omega,t) = \frac{1}{4}\left|\sum_i r_i(t)(\tilde{d}_i(\Omega,t) - \tilde{d}_g(\Omega))\right|^2 . \tag{7}$$

A complete theoretical description of TRHHS experiments of the photodissociation of CH_3I according to the above equations would require 9-dimensional potential energy surfaces of the $^3Q_{0^+}$, $^1Q_1$ and $^3Q_1$ states of the neutral molecule and the $\widetilde{X}^+$, $\widetilde{A}^+$ and $\widetilde{B}^+$ states of the cation and 9-dimensional non-adiabatic wave packet calculations. Dyson orbitals, strong-field ionisation rates and photorecombination matrix elements [20, 49, 50] would then be needed for the molecular geometries relevant to the dissociation pathway to finally provide the expected high-harmonic signals. Although 9-dimensional wave-packet calculations have recently been reported [51], the calculation of the other required quantities is currently an active area of research [52–56].

We therefore turn to a much simpler theoretical model that only takes into account the variation of the high-harmonic phase along the dissociation pathway [15]. High-harmonic transient grating spectroscopy has indeed been shown to be much more sensitive to phase than to amplitude modulations [57]. A quantitative derivation of the diffraction efficiencies of high-harmonic phase and amplitude gratings has been given in Ref. [10]. We further simplify the excited-state dynamics to wave packet propagation on the $^3Q_{0^+}$ electronically excited state only, given that it accounts for up to 90% of the excited-state population [24, 26]. In the case of CF_3I, between 88 and 100 % of the atomic iodine fragments are produced in the $^2P_{1/2}$ state [58, 59].

Equations (6) and (7) are therefore simplified by replacing the sum over i with a single electronically excited state (the $^3Q_{0^+}$ state) designated with the subscript e and we use the same normalisation as in the experimental results, i.e. we factorize out the emission intensity of the unexcited molecules and define $\tilde{d}_e(\Omega,t) = \tilde{d}_i(\Omega,t)/\tilde{d}_g(\Omega)$. In our calculations we thus use the expressions

$$I_{m=0}(\Omega,t) = \left|\tilde{d}_g(\Omega)\right|^2 \left|1 - r(t) + r(t)\tilde{d}_e(\Omega,t)\right|^2 \tag{8}$$

$$I_{m=\pm1}(\Omega,t) = \left|\tilde{d}_g(\Omega)\right|^2 \frac{r(t)^2}{4}\left|\tilde{d}_e(\Omega,t) - 1\right|^2 , \tag{9}$$

where

$$\tilde{d}_e(\Omega, t) = \int \mathrm{d}\mathbf{R} |\chi_e(\mathbf{R}, t)|^2 e^{-i(\phi_{\mathrm{tot},e}(\mathbf{R},\Omega) - \phi_{\mathrm{tot},g}(\Omega))}. \quad (10)$$

These expressions are evaluated using nuclear wave packets $\chi_e(\mathbf{R}, t)$ obtained by solving the one-dimensional time-dependent Schrödinger equation using the split-operator technique [60] along the dissociation pathway on the $^3Q_{0^+}$ surface. We include the explicit interaction with a 50-fs resonant photoexcitation pulse, but neglect the temporal broadening imparted by the probe pulse. Our wave packet calculations use a temporal step of 50 as and a grid with a spatial step of 0.007 Å. The potential energy curve of the $^3Q_{0^+}$ state as a function of the C-I bond length with all other internal coordinates relaxed was taken from Ref. [39]. The time-dependent wave packet and the potential energy curves shown in Fig. 5 serve as input to calculate the high-harmonic intensities according to Eqs. (8-10).

The results of these calculations, shown in Fig. 6, reproduce the qualitative temporal evolution of all measured signals and reflect all observed trends. The signal in $m = 0$ is observed to decrease during excitation and to subsequently recover to an asymptotic level that decreases with increasing high-harmonic order. The diffracted signal ($m = \pm 1$) is found to increase during excitation to reach a maximum that increases with harmonic order and is delayed with respect to zero time delay. The diffracted signal subsequently decays to an asymptotic value that also increases with harmonic order. These observations are all in good agreement with the experimental data shown in Fig. 3. Moreover, the relative intensity of the diffracted radiation in the range of 2–10×10^{-3} is in quantitative agreement with the experiment. We thus conclude that the variation of the high-harmonic phase along the dissociation pathway is one of the dominant effects probed by the experiment. The most significant discrepancy between experiment and theory is the time scale of the signal variations which is slower in the experimental than in the theoretical results. A fitting procedure of Eqs. (1) and (2) to the theoretical results shown in Fig. 6 provides an excellent reproduction of the calculated curves with exponential time constants that are however much shorter than those observed in the experiment. A similar result has been previously obtained in studies of the photodissociation of Br_2 [16]. We discuss and interpret this result in the following section.

The theoretical model presented here is extremely simplified because it considers only one dimension of the wave-packet motion, it includes only the $^3Q_{0^+}$ state of the neutral molecule and the $\widetilde{X}^+\ ^2E_{3/2}$ state of the cation and finally, it ignores also the variation of both the ionization rate and the photorecombination matrix elements with the molecular geometry. Nevertheless, this simple model reproduces the main features of the experiment, both the qualitative variation of the measured intensities and the trends in the observed signal levels. Our time-dependent wave packet in the $^3Q_{0^+}$ state is in good agreement with the results of a 4-dimensional calculation reported in Ref. [26]. In the future, our model will be improved by performing wave packet calculations in higher, ideally full dimensionality (9D) as recently reported [51], calculating strong-field ionisation rates and photorecombination matrix elements for the relevant geometries and extending the model to include the lowest-lying electronic states of the cation. According to detailed calculations of the potential energy surfaces of the cation, excited electronic states will almost certainly play a role in the region of C-I internuclear separations above 4 Å where the $\widetilde{X}^+$, $\widetilde{A}^+$ and $\widetilde{B}^+$ states intersect and lie within 2 eV of the $\widetilde{X}^+$ electronic ground state of the cation [46].

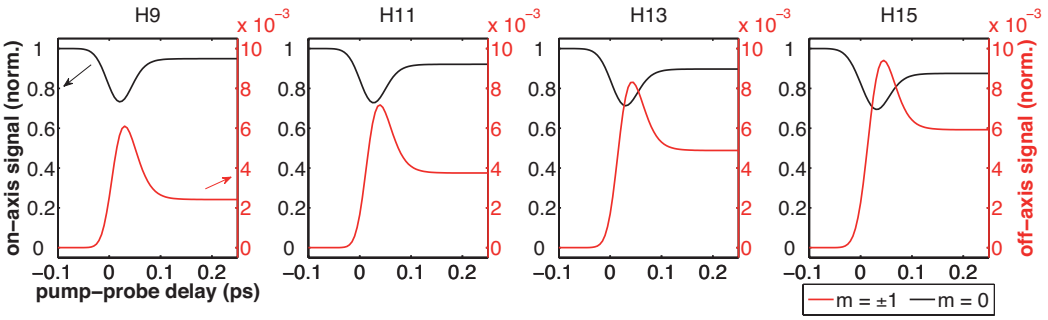

Figure 6. normalised calculated high-harmonic intensities in $m = 0$ and $m = \pm 1$ for CH_3I according to the theoretical model described in the text using a pump pulse of 50-fs duration centered at 267 nm and a peak intensity of the probe pulse of $1.5{\times}10^{14}$W/cm^2. The nuclear wave packet is taken from a one-dimensional propagation on the $^3Q_{0^+}$ surface and strong-field ionisation to the $\tilde{X}\,^2E_{3/2}$ surface of the cation is included in the calculation.

5. Discussion

The time constants obtained from the present experiments on the photodissociation of CH_3I overlap with the 125 fs measured by Zewail and co-workers using time-resolved KETOF spectroscopy [25]. That technique measures the appearance of a fragment as a step function, the centre of which is defined as the appearance time. In contrast TRHHS measures the variation of the high-harmonic signal of a transient species until it reaches the asymptotic signal level. The KETOF technique relies on resonant few-photon ionisation of the fragments. It therefore measures the time scale on which the nascent fragment develops the electronic absorption spectrum of the isolated fragment. Along the same reasoning, TRHHS can be described as measuring the time scale on which the transient species develop the high-harmonic emission spectrum of the isolated fragments. In the case of CH_3I, our results thus suggest that the time scale for the development of the high-harmonic emission spectra of the isolated fragments is consistent overall with the development of the absorption spectra of isolated fragments. This result is intuitive considering that high-harmonic generation is an electronic process which is therefore particularly sensitive to the electronic structure of the molecules. The similar time scales extracted from KETOF and TRHH spectroscopies can thus be rationalised as the time scales for the development of the electronic structure of the free fragments.

The comparison of our experimental and theoretical results shows that the effect of the coordinate-dependent ionisation potential on the phase of the high-harmonic emission is very pronounced and qualitatively explains the main observations. However, the time scales for the development of the isolated fragment emission are slower in the experiment than in the calculations. Moreover, although the time constants determined for different harmonic orders overlap within 1 standard deviation, a systematic trend of increasing time constants is observed with increasing order. A similar result has previously been obtained in Br_2, but the time constants were not determined [15]. The present observations suggest a variation of the photorecombination matrix elements that extends to large dissociation coordinates. The weak order dependence of the time constants could originate from a higher sensitivity of the photorecombination matrix element to the nuclear configuration, as might be expected from the shorter de-Broglie wavelength of the recombining electron.

In addition, the slower time scale of the experiment and the weak order dependence could also be related to the presence of photofragments within the extension of the continuum electron trajectories that range from 1.6 Å for H9 to 4.5 Å for

H15 under the conditions of the present experiment. These effects should however be small in the experiments reported here because the electron trajectories mainly unfold perpendicular to the C-I axis.

6. Conclusions and Outlook

We have applied time-resolved high-harmonic spectroscopy to the photodissociation of CH_3I and CF_3I following excitation to their respective A bands. Time constants for the development of the high-harmonic spectra of the free fragments have been determined. In the case of CH_3I, the time constants are consistent with the time scale of appearance of the methyl fragment determined by the KETOF method [25]. The global temporal variation of the observed signals has been explained in terms of the variation of the vertical ionisation potential along the reaction pathway. This simple model however underestimates the observed time scales. A weak dependence of the time constants on the harmonic order was observed and tentatively attributed to an order-dependent sensitivity of the photorecombination matrix elements to the nuclear configuration. In the case of CF_3I, we have reported the first time-resolved measurement of the A-band photodissociation. The time constants measured by high-harmonic spectroscopy fall within the 150-350 fs interval for the photodissociation time inferred from fragment anisotropies in Ref. [30]. In the near future, the temporal resolution of the experiment will be improved using temporally compressed 267 nm pulses to study the dynamics at the conical intersection that is expected to be reached $\sim$20 fs after photoexcitation. The measurements will also be extended to oriented CH_3I molecules [11], which should reveal the time scale on which the molecular asymmetry is lost along the dissociation pathway leading to planar CH_3 and atomic iodine.

Acknowledgments

We gratefully acknowledge funding from the Swiss National Science Foundation (PP00P2_128274) and ETH Zürich (ETH-33 10-3).

References

[1] M. Drescher, M. Hentschel, R. Kienberger, M. Uiberacker, V. Yakovlev, A. Scrinzi, T. Westerwalbesloh, U. Kleineberg, U. Heinzmann and F. Krausz, Nature **419**, 803 (2002).
[2] J. Mauritsson, P. Johnsson, E. Mansten, M. Swoboda, T. Ruchon, A. L'Huillier and K.J. Schafer, Phys. Rev. Lett. **100**, 73003 (2008).
[3] G. Sansone, F. Kelkensberg, J.F. Pérez-Torres, F. Morales, M.F. Kling, W. Siu, O. Ghafur, P. Johnsson, M. Swoboda, E. Benedetti, F. Ferrari, F. Lépine, J.L. Sanz-Vicario, S. Zherebtsov, I. Znakovskaya, A. L'Huillier, M.Y. Ivanov, M. Nisoli, F. Martín and M.J.J. Vrakking, Nature **465**, 763 (2010).
[4] L. Nugent-Glandorf, M. Scheer, D.A. Samuels, A.M. Mulhisen, E.R. Grant, X. Yang, V.M. Bierbaum and S.R. Leone, Phys. Rev. Lett. **87** (19), 193002 (2001).
[5] P. Wernet, M. Odelius, K. Godehusen, J. Gaudin, O. Schwarzkopf and W. Eberhardt, Phys. Rev. Lett. **103** (1), 013001 (2009).
[6] J. Itatani, J. Levesque, D. Zeidler, H. Niikura, H. Pépin, J.C. Kieffer, P.B. Corkum and D.M. Villeneuve, Nature **432**, 867 (2004).
[7] T. Kanai, S. Minemoto and H. Sakai, Nature **435** (7041), 470 (2005).
[8] X. Zhou, R. Lock, W. Li, N. Wagner, M.M. Murnane and H.C. Kapteyn, Phys. Rev. Lett. **100** (7), 073902 (2008).
[9] C. Vozzi, M. Negro, F. Calegari, G. Sansone, M. Nisoli, S. De Silvestri and S. Stagira, Nat Phys **7** (10), 822 (2011).

[10] A. Rupenyan, J.B. Bertrand, D.M. Villeneuve and H.J. Wörner, Phys. Rev. Lett. **108** (3), 033903 (2012).
[11] P.M. Kraus, A. Rupenyan and H.J. Wörner, Phys. Rev. Lett. **109**, 233903 (2012).
[12] A. Rupenyan, P.M. Kraus, J. Schneider and H.J. Wörner, Phys. Rev. A, accepted (2013).
[13] N.L. Wagner, A. Wüest, I.P. Christov, T. Popmintchev, X. Zhou, M.M. Murnane and H.C. Kapteyn, Proc. Natl. Acad. Sci. USA **103**, 13279 (2006).
[14] W. Li, X. Zhou, R. Lock, S. Patchkovskii, A. Stolow, H.C. Kapteyn and M.M. Murnane, Science **322** (5905), 1207 (2008).
[15] H.J. Wörner, J.B. Bertrand, D.V. Kartashov, P.B. Corkum and D.M. Villeneuve, Nature **466** (7306), 604 (2010).
[16] H.J. Wörner, J.B. Bertrand, P.B. Corkum and D.M. Villeneuve, Phys. Rev. Lett. **105** (10), 103002 (2010).
[17] M.D. Fayer, Annu. Rev. Phys. Chem. **33**, 63 (1982).
[18] S. Mukamel, *Principles of Nonlinear Optical Spectroscopy* (Oxford University Press, New York, 1999).
[19] Y. Mairesse, D. Zeidler, N. Dudovich, M. Spanner, J. Levesque, D.M. Villeneuve and P.B. Corkum, Phys. Rev. Lett. **100**, 143903 (2008).
[20] H.J. Wörner, J.B. Bertrand, B. Fabre, J. Higuet, H. Ruf, A. Dubrouil, S. Patchkovskii, M. Spanner, Y. Mairesse, V. Blanchet, E. Mével, E. Constant, P.B. Corkum and D.M. Villeneuve, Science **334** (6053), 208 (2011).
[21] P.M. Kraus and H.J. Wörner, Chem. Phys. in press, doi: 10.1016/j.chemphys.2012.01.013 (2012).
[22] P.M. Kraus, Y. Arasaki, J.B. Bertrand, S. Patchkovskii, P.B. Corkum, D.M. Villeneuve, K. Takatsuka and H.J. Wörner, Phys. Rev. A **85**, 043409 (2012).
[23] J.V.V. Kasper and G.C. Pimentel, Appl. Phys. Lett. **5**, 231 (1964).
[24] A.T.J.B. Eppink and D.H. Parker, J. Chem. Phys. **109**, 4758 (1998).
[25] D. Zhong and A.H. Zewail, J. Phys. Chem. A **102**, 4031 (1998).
[26] R. de Nalda, J. Durá, A. García-Vela, J.G. Izquierdo, J. González-Vázquez and L. Bañares, J. Chem. Phys. **128**, 244309 (2008).
[27] J. Durá, R. de Nalda, G.A. Amaral and L. Bañares, J. Chem. Phys. **131**, 134311 (2009).
[28] V.N. Krylov, M.V. Nikitchenko, M. Quack and G. Seyfang, Proc. SPIE **5337**, 178 (2004).
[29] V.N. Krylov, A. Kushnarenko, E. Miloglyadov, M. Quack and G. Seyfang, Proc. SPIE **6460**, 26 (2007).
[30] Y.S. Kim, W.K. Kang and K.H. Jung, J. Chem. Phys. **105**, 551 (1996).
[31] W.G. Roeterdink and M.H.M. Janssen, Phys. Chem. Chem. Phys. **4**, 601 (2002).
[32] W.G. Roeterdink and M.H.M. Janssen, Chem. Phys. Lett. **345**, 72 (2001).
[33] Y. He, M. Quack, R. Ranz and G. Seyfang, Chem. Phys. Lett. **215**, 228 (1993).
[34] E. Hamilton, T. Seideman, T. Ejdrup, M.D. Poulsen, C.Z. Bisgaard, S.S. Viftrup and H. Stapelfeldt, Phys. Rev. A **72**, 43402 (2005).
[35] J.B. Bertrand, H.J. Wörner, H.C. Bandulet, E. Bisson, M. Spanner, J.C. Kieffer, D.M. Villeneuve and P.B. Corkum, Phys. Rev. Lett. **106**, 023001 (2011).
[36] R.S. Mulliken, J. Chem. Phys. **8**, 382 (1940).
[37] T.F. Hunter and K.S. Kristjansson, Chem. Phys. Lett. **58**, 291 (1978).
[38] A.T.J.B. Eppink and D.H. Parker, J. Chem. Phys. **110**, 832 (1999).
[39] A.B. Alekseyev, H.P. Liebermann, R.J. Buenker and S.N. Yurchenko, J. Chem. Phys. **126**, 234102 (2007).
[40] A.B. Alekseyev, H.P. Liebermann and R.J. Buenker, J. Chem. Phys. **134**, 044303 (2011).
[41] Y.J. Bae and M.S. Kim, ChemPhysChem **9**, 1709 (2008).
[42] B. Urban and V.E. Bondybey, J. Chem. Phys. **116**, 4938 (2002).
[43] Y. Song, X.M. Qian, K.C. Lau, C.Y. Ng, J. Liu and W. Chen, J. Chem. Phys. **115**, 4095 (2001).
[44] M. Grütter, J.M. Michaud and F. Merkt, J. Chem. Phys. **134**, 4308 (2011).
[45] K. Walter, R. Weinkauf, U. Boesl and E.W. Schlag, J. Chem. Phys. **89**, 1914 (1988).
[46] R. Locht, D. Dehareng, K. Hottmann, H.W. Jochims, H. Baumgärtel and B. Leyh, J. Phys. B **43**, 5101 (2010).
[47] M. Lewenstein, P. Balcou, M.Y. Ivanov, A. L'Huillier and P. Corkum, Phys. Rev. A **49**, 2117 (1994).
[48] T. Kanai, E.J. Takahashi, Y. Nabekawa and K. Midorikawa, Phys. Rev. Lett. **98**, 153904 (2007).
[49] S. Patchkovskii, Z. Zhao, T. Brabec and D.M. Villeneuve, Phys. Rev. Lett. **97**, 123003 (2006).
[50] M. Spanner and S. Patchkovskii, Phys. Rev. A **80**, 063411 (2009).
[51] C.R. Evenhuis and U. Manthe, J. Phys. Chem. A **115**, 5992 (2011).

[52] R. Murray, M. Spanner, S. Patchkovskii and M.Y. Ivanov, Phys. Rev. Lett. **106**, 173001 (2011).
[53] A.T. Le, T. Morishita, R.R. Lucchese and C.D. Lin, Phys. Rev. Lett. **109**, 203004 (2012).
[54] O.I. Tolstikhin, T. Morishita and L.B. Madsen, Phys. Rev. A **84**, 53423 (2011).
[55] L.B. Madsen, O.I. Tolstikhin and T. Morishita, Phys. Rev. A **85**, 53404 (2012).
[56] L. Torlina, M. Ivanov, Z.B. Walters and O. Smirnova, Phys. Rev. A **86**, 43409 (2012).
[57] H.J. Eichler, P. Günter and D.W. Pohl, *Laser-induced dynamic gratings* (Springer, Berlin, 1986).
[58] P. Felder, Chem. Phys. **155**, 435 (1991).
[59] A. Furlan, T. Gejo and J.R. Huber, J. Phys. Chem. **100**, 7956 (1996).
[60] D.J. Tannor, *Introduction to Quantum Mechanics: A Time-Dependent Perspective* (University Science Books, Sausalito, 2007).